# Evolution of tidal system and bottom stress in the East China Seas since the Last Glacial Maximum

Wenxin Liu, Jie Shi

Ocean University of China, Qingdao, 266100, China

# 1 Purposes

Global mean sea level has risen continuously, reaching a record high in 2024. From the Last Glacial Maximum (LGM, ~20 ka BP) to ~6 ka BP, sea level rose from -130 m to modern levels (Yokoyama et al., 2019). The East China Seas (ECSs) were largely subaerially exposed during the LGM. Sea level rise critically influenced ECSs tidal regimes, where the M<sub>2</sub> tide dominates sediment transport (Uehara et al., 2002). Existing paleo-tidal reconstructions focus solely on sea level changes, neglecting boundary condition adjustments necessary for realistic simulations. Key unknowns include paleo-tidal impacts on seabed stress evolution and sediment dispersal.

This study refines ECSs paleo-tidal reconstructions by integrating global simulation data to adjust open boundary conditions, enabling accurate tidal regime modeling. By analyzing tidal-induced bottom stress variations, we aim to unravel sediment migration patterns under paleo-hydrodynamic forcing, advancing predictions of shelf sedimentary responses to sea level changes.

#### 2 Methods

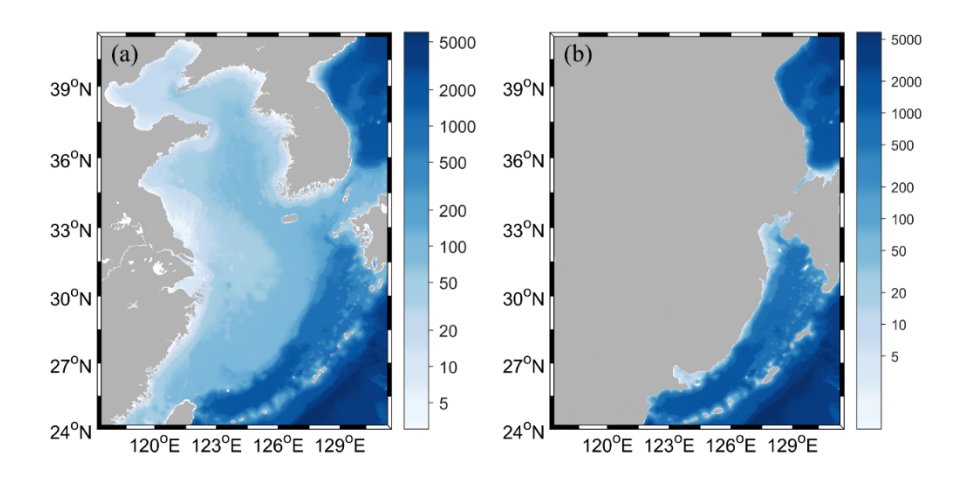


Fig. 1. Schematic of water depths in the ECSs, where (a) represents the present-day sea level, and (b) represents a sea level drop to -130 meters.

The two-dimensional hydrodynamic model employed in this study is based on the Princeton Ocean Model (POM), configured with a horizontal resolution of 1/18° (~5 km). The computational

domain spans the East China Seas (ECSs; 117.5°–131.5°E, 24°–41°N). A cold-start initialization is implemented, with open boundaries forced by paleo-tidal constituents (M<sub>2</sub>, S<sub>2</sub>, K<sub>1</sub>, O<sub>1</sub>). The harmonic constants for these constituents are derived from the TiME (Tidal Model Forced by Ephemerides) paleo-tidal model developed by Sulzbach et al. (2023), with sea level adjustments corresponding to distinct historical periods.

In the paleo-oceanographic numerical experiments, sea level is reduced to -130 m during the LGM, contrasting with the modern baseline (0 m experiment). For the open boundary experiments, the lowered sea level is reconfigured while maintaining tidal boundary conditions consistent with contemporary values.

#### 3 Results

### 3.1 Evolution of tidal Systems

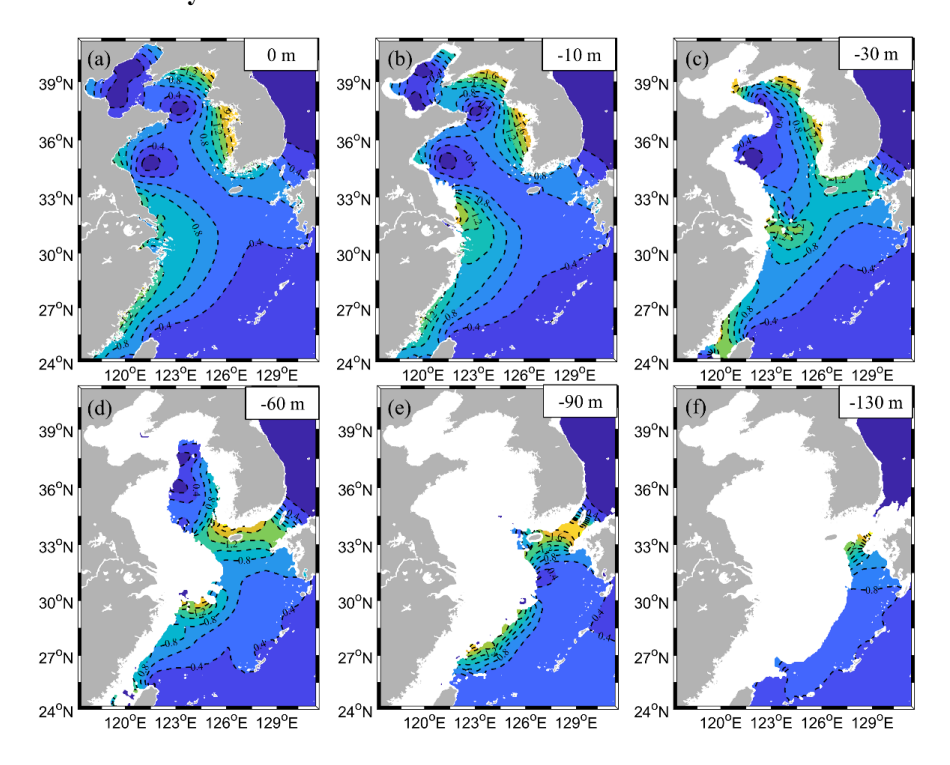


Fig. 2. Co-amplitude lines of  $M_2$  in the ECSs corresponds to the different sea level lowering.

The spatial distribution of  $M_2$  tidal constituent amplitudes in the ECSs under varying sea level scenarios is illustrated in Figure 2. As sea level is lowered to -10 m, the amphidromic points in the Bohai Sea begins to degenerate. At -30 m, the two amphidromic points in the Yellow Sea exhibit degeneration, with significantly amplified tidal amplitudes along the western coast of the Korean Peninsula. Further sea level reduction leads to the formation of a semi-enclosed embayment in the

northern Yellow Sea. At -60 m, the Yellow Sea embayment contracts, accompanied by continued degeneration of amphidromic points and eastward progradation of the East China Sea coastline. By -90 m, the co-tidal chart simplifies markedly, reflecting reduced tidal complexity. Subsequent sea level lowering triggers the closure of the Tsushima Strait.

Mechanistically, sea level fluctuations alter tidal regimes primarily through bathymetric geometry modifications, which modulate tidal wavelength and resonance conditions. These changes drive systematic shifts in amphidromic point stability and tidal energy distribution across the ECSs.

# 3.2 Analysis of tidal-induced bottom shear stress evolution in the ECSs

The monthly maximum tidal-induced bottom shear stress ( $\tau$ ) distribution in the modern ECSs is illustrated in Figure 3a. A comparison with sediment grain size distributions reveals strong spatial correlations. The  $0.35~\text{N/m}^2~\tau$  contour aligns approximately with the margins of muddy deposits in the Bohai Sea and central Yellow Sea(Uehara et al., 2002). Similarly, regions with  $\tau \geq 1.50~\text{N/m}^2$  in the southern Yellow Sea correspond well with sand ridge distributions(Zhou et al., 2016). However, tidal forcing alone cannot fully explain sedimentary patterns across most of the East China Sea shelf, necessitating future incorporation of mean currents into the model framework.

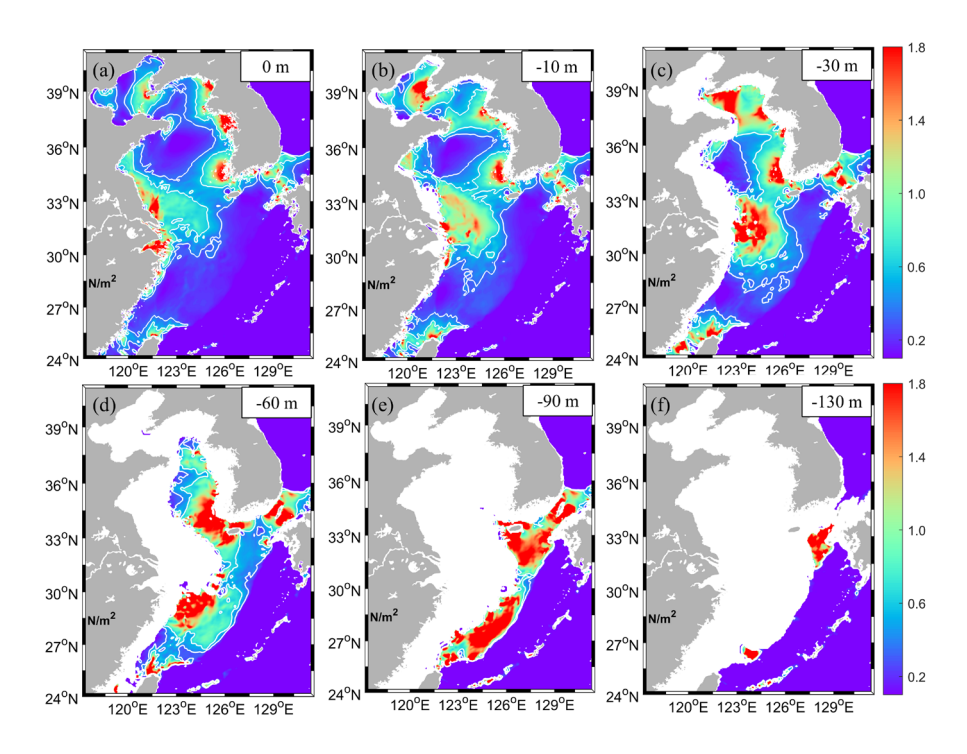


Fig. 3. Evolutionary characteristics of the maximum bottom stress driven by tidal forcing in the ECSs corresponds to the different sea level lowering.

When the mean sea level is lowered to between -10 m and -30 m, high bed shear stress ( $\tau > 1.5$  N/m²) dominates the outer shelf near the Yangtze River estuary, indicating intensified tidal forcing during this period. Minimal  $\tau$  values in the northern and southern Yellow Sea coincide spatially with amphidromic points, consistent with reduced tidal energy dissipation. Regions of elevated  $\tau$  likely play a critical role in tidal sand ridge formation. At lower sea levels (-60 m to -130 m),  $\tau$  exceeding 1.5 N/m² expands across the East China Sea shelf, near Jeju Island, and through the Tsushima Strait. Enhanced  $\tau$  magnitudes and spatial extents in shallow areas suggest amplified tidal currents and greater seabed reworking during low stand conditions, likely attributed to heightened tidal resonance over the exposed continental shelf.

#### 3.3 Impact of open boundary conditions on tidal-induced bottom shear stress distribution

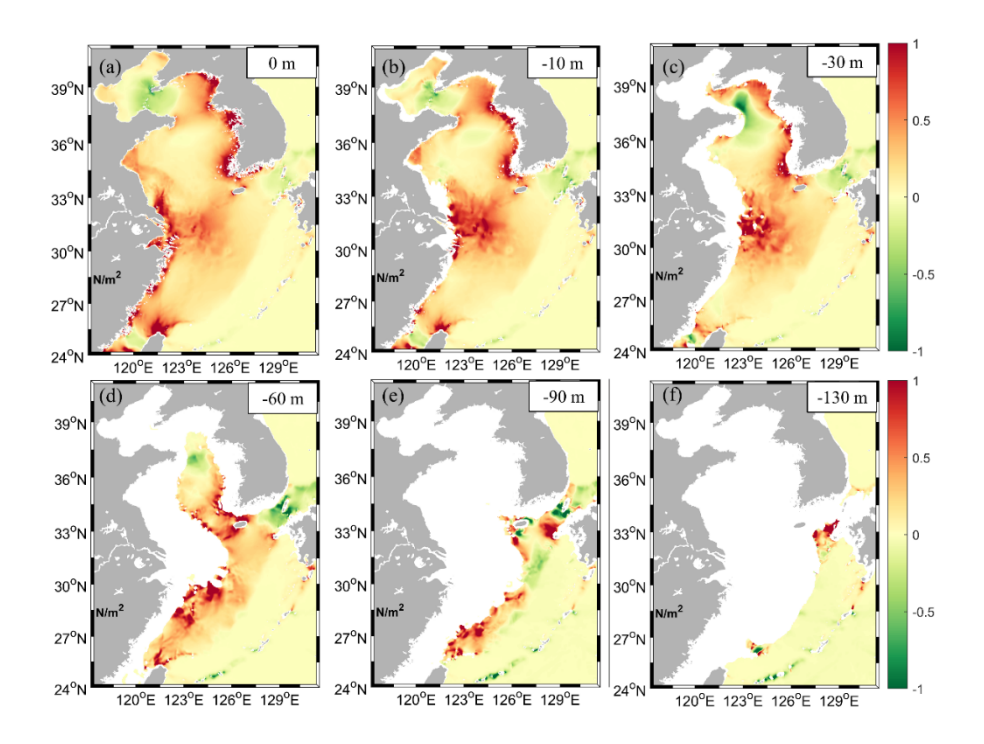


Fig. 4. Effects of different open boundary conditions of the maximum bottom stress driven by tidal forcing in the ECSs.

Figure 4 illustrates the difference in monthly maximum bed shear stress (τ) within the ECSs under two tidal boundary condition scenarios: Case1: All sea level experiments adopt the modern NAO.99b tidal dataset (Matsumoto et al., 2000) at open boundaries, maintaining consistent tidal forcing.Case2: Open boundaries are forced by paleo-tidal data from the TiME model (Sulzbach et

al.), which provides global tidal reconstructions interpolated for corresponding historical periods (as described in preceding results).

Spatial differences in  $\tau$  between the two cases are generally minor across most regions. Under modern sea level (0 m), Case1 generates stronger tidal currents in the southern boundary (Taiwan Strait), with higher near-shore velocities compared to Case2, whereas weaker currents prevail in the Bohai Sea. Under lowered sea levels, Case1 exhibits enhanced tidal currents near the Yangtze Estuary and coastal zones, though these discrepancies gradually diminish with further sea level reduction. This suggests that the influence of boundary conditions on seabed stress magnitudes weakens as sea level declines, likely due to reduced tidal resonance and altered amphidromic systems under paleogeographic configurations.

# 4 Future Challenges

Future studies will integrate wind stress, mean currents, and additional hydrodynamic forcings into the numerical framework to refine the understanding of paleo-oceanographic dynamic controls on seabed stress evolution and sediment transport pathways. These enhancements aim to elucidate the synergistic effects of multi-scale forcings on sedimentary dynamics under varying paleo-environmental conditions..

## Reference

Sulzbach, R., Klemann, V., Knorr, G., Dobslaw, H., Dümpelmann, H., Lohmann, G., & Thomas, M. (2023). Evolution of global ocean tide levels since the Last Glacial Maximum. *Paleoceanography and Paleoclimatology*, 38(5), e2022PA004556.

Uehara, K., Saito, Y., & Hori, K. (2002). Paleotidal regime in the Changjiang (Yangtze) Estuary, the East China Sea, and the Yellow Sea at 6 ka and 10 ka estimated from a numerical model. *Marine Geology*, 183(1-4), 179-192.

Yokoyama, Y., Purcell, A., & Ishiwa, T. (2019). Gauging quaternary sea level changes through scientific ocean drilling. *Oceanography*, *32*(1), 64-71.

Zhou, C., Zheng, J., Dong, P., Zhang, J., Zhu, Y., & Zhang, Z. (2016). Tidal evolution in the Yellow and East China Sea during holocene. *Journal of Coastal Research*, (75), 785-789.